

Synthesis, physicochemical characterization, geometric structure and molecular docking of new biologically active ferrocene based Schiff base ligand with transition metal ions

W.H. Mahmoud | N.F. Mahmoud | Gehad G. Mohamed 

Chemistry Department, Faculty of Science,
Cairo University, Giza 12613, Egypt

Correspondence

Gehad G. Mohamed, Chemistry Department,
Faculty of Science, Cairo University, Giza,
12613, Egypt.

Email: ggenidymohamed@sci.cu.edu.eg

Physicochemical studies were performed to study new ferrocene based Schiff base ligand (HL), (Z)-4-(1-((2-carboxycyclohexa-2,4-dien-1-yl)imino)ethyl) [bis(η^5 cyclopenta-1,3-dien-1 yl)]iron with some transition metal ions to form a series of ferrocenyl derivatives bearing transition metal complexes of the type $[M(L)Cl(H_2O)_3]$ ($M = Ni(II), Cu(II)$), $[M(L)Cl(H_2O)_3]nH_2O$ ($M = Mn(II)$ ($n = 1$), $Co(II)$ ($n = 1$), $Zn(II)$ ($n = 2$) and $Cd(II)$ ($n = 3$)) and $[M(L)Cl(H_2O)_3]Cl.nH_2O$ ($M = Cr(III)$ ($n = 2$) and $Fe(III)$ ($n = 1$)). The new ligand and metal ion complexes have been prepared and characterized by IR, UV-Vis, 1H -NMR, TG/DTA, elemental analysis and mass spectrometry. The TGA/DTG analysis revealed that the ferrocene precursors decompose spontaneously to form iron(II) oxide. The molecular and electronic structure of the ligand (HL) was optimized theoretically and the quantum chemical parameters were calculated. The molecular structure with a variety of functionalities can be used to investigate the coordination sites and the total charge density around each atom. DFT-based molecular orbital energy calculations of the new ligand have been also studied. All of the complexes were screened against a panel of Gram (+) bacteria: *Streptococcus pneumoniae* and *Bacillus subtilis*, Gram (-) bacteria: *Pseudomonas aeruginosa* and *Escherichia coli* and panel of fungi: *Aspergillus fumigatu*, *Syncephalastrum racemosum*, *Geotricum candidum* and *Candida albicans*. Anticancer activity screening for the tested compounds using 4 different concentrations of HL ligand against human tumor cells of breast cancer cell line MCF-7 were obtained. Molecular docking was used to predict the binding between HL ligand and human-DNA-Topo I complex (PDB ID: 1SC7), the receptors of breast cancer mutant oxidoreductase (PDB ID: 3HB5), crystal structure of *Escherichia coli* (PDB ID: 3T88), to identify the binding mode and the crucial functional groups interacting with the three proteins.

KEYWORDS

bacteria, breast cancer, DFT, Docking, ferrocene Schiff base, physicochemical studies, TGA/DTG

1 | INTRODUCTION

Metal containing or organometallic compounds are much sought after in recent years.^[1,2] Ferrocene, the archetypal

organometallic compound, is of interest for fundamental reasons, such as bonding and structure, and its numerous, diverse, potential applications.^[3] Ferrocene compounds have interesting redox properties and they are used in catalytic

reactions. They have many potential medicinal applications as therapeutic agents in the new field of bioorganometallics, including as anti-cancer, anti tubercular and anti-fungal agents among many others.^[4] Ferrocene has garnered interest over the years as the ubiquitous group to append onto other active molecules in order to favorably modify the properties of already active compounds. This has been done with great success in many cases as several important compounds have been synthesized and tested in such a manner.^[5] Acetylferrocene is the organo iron compound with the formula $[(C_5H_5)Fe(C_5H_4COMe)]$, (where Me: methyl). It consists of ferrocene substituted by an acetyl group on one of the cyclopentadienyl rings. It is an orange, air-stable solid that is soluble in organic solvents. Acetylferrocene is prepared by Friedel-Crafts acylation of ferrocene, usually with acetic anhydride. Acetylferrocene can be converted to many derivatives, e.g. reduction to the chiral alcohol $[(C_5H_5)Fe(C_5H_4CH(OH)Me)]$ and precursor to vinylferrocene. The oxidized derivative, acetylferrocenium, is used as a $1e^-$ -oxidant in the research laboratory.^[6] Functionalized ferrocenes play diverse roles in modern chemistry, with systems featuring pendant Lewis basic groups acting as donor ligands in various complexes exploited in homogenous catalysis, and those bearing Lewis acidic groups finding applications, for example, in polymer synthesis and in detection/sensing. The latter field exploits cathodic shifts in the redox potential of the Fe(II) centre which can be induced, for example, on coordination of a Lewis base to a transition metal ion.^[7–9] Ferrocene is a highly redox-active organometallic substance, which has been employed as magnetic, optical, and electrochemical materials. Also, chemical modification through organic synthesis enabled the synthesis of various ferrocene derivatives and ferrocene-containing polymers^[10,11] The coordination chemistry of the complexes involving Schiff base ligands having O and N donor atoms and a number of transition metal ions has become area of much focus due to the versatility of Schiff base ligands on treating with transition metal ions produces mono as well as polynuclear complexes, which have been widely employed in material science and medicine. The Schiff base complexes may incorporate planar aromatic or flexible polydentate ligands.^[12] The present study described the coordination behavior of **(Z)-4-(1-((2-carboxycyclohexa-2,4-dien-1-yl)imino)ethyl)-[bis(η^5 -cyclopenta-1,3-dien-1-yl)]iron** (HL ligand) (Figure 1) toward some transition elements. Metal(II)/(III) complexes of the new HL ligand was focused and its in vitro antibacterial, antifungal and anticancer activity were investigated. The structure of the studied bi- and trivalent metal complexes of HL ligand is elucidated using elemental analyses, IR, 1H NMR, mass spectroscopy, molar conductance, magnetic susceptibility and thermal analyses measurements.^[13] The molecular docking study was described in order to elucidate the mode of binding between the ferrocene Schiff

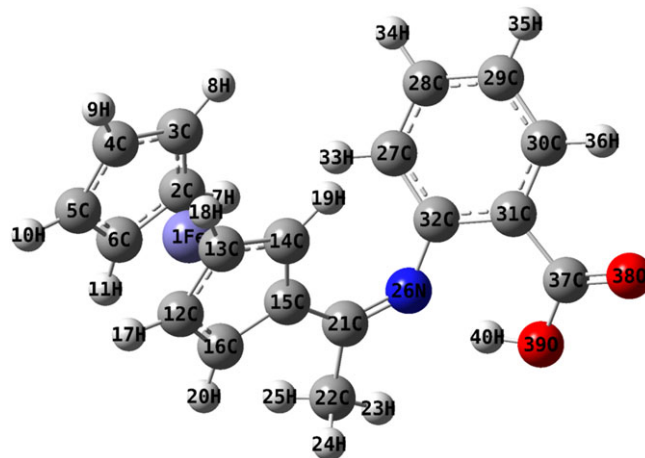


FIGURE 1 The optimized structure of HL ligand

base ligand and human-DNA-Topo I complex (PDB ID: 1SC7), the receptors of breast cancer mutant oxidoreductase (PDB ID: 3HB5) and crystal structure of *Escherichia coli* (PDB ID: 3 T88). The antimicrobial and anticancer activities were screened.

2 | EXPERIMENTAL

2.1 | Material and reagent

All chemicals used were of the analytical reagent grade (AR), and of highest purity available. The chemicals used included acetyl ferrocene which was supplied from Strem Chemicals Inc., $CrCl_3 \cdot 6H_2O$ and $MnCl_2 \cdot 2H_2O$ (Sigma Aldrich), $NiCl_2 \cdot 6H_2O$, $CoCl_2 \cdot 6H_2O$, $CuCl_2 \cdot 2H_2O$ and $ZnCl_2 \cdot 2H_2O$ (BDH), $FeCl_3 \cdot 6H_2O$ (Prolabo), $CdCl_2 \cdot 2H_2O$ (Merck) and anthranilic acid (BDH). Organic solvents were spectroscopic pure from BDH included ethanol, diethyl ether and dimethyl formamide. Hydrogen peroxide, sodium chloride, sodium carbonate and sodium hydroxide (A.R.) were used. Human tumor cell line (Breast cell) was obtained frozen in liquid nitrogen ($-180^\circ C$) from the American Type Culture Collection. The tumor cell line (MCF7) was maintained in the National Cancer Institute, Cairo, Egypt, by serial sub-culturing.

2.2 | Solutions

A fresh stock solution of 1×10^{-3} M of acetyl ferrocene (0.4 g/L) was prepared in the appropriate volume of absolute ethanol and metanol. Dimethylsulphoxide (DMSO) (Sigma Chemical Co., St. Louis, Mo, USA): It was used in cryopreservation of cells. RPMI-1640 medium (Sigma Chemical Co., St. Louis, Mo, USA) was used. The medium was used for culturing and maintenance of the human tumor cell lines. The medium was supplied in a powder form. It was prepared as follows: 10.4 g medium was weighed, mixed with 2 g

sodium bicarbonate, completed to 1 l with distilled water and shook carefully till complete dissolution. The medium was then sterilized by filtration in a Millipore bacterial filter (0.22 μm). The prepared medium was kept in a refrigerator (4 $^{\circ}\text{C}$) and checked at regular intervals for contamination. Before use the medium was warmed at 37 $^{\circ}\text{C}$ in a water bath and the supplemented with penicillin/streptomycin and FBS. Sodium bicarbonate (Sigma Chemical Co., St. Louis, Mo, USA) was used for the preparation of RPMI-1640 medium. 0.05% isotonic Trypan blue solution (Sigma Chemical Co., St. Louis, Mo, USA) was prepared in normal saline and was used for viability counting. 10% Fetal Bovine Serum (FBS) (heat inactivated at 56 $^{\circ}\text{C}$ for 30 min), 100 units/ml Penicillin and 2 mg/ml Streptomycin were supplied from Sigma Chemical Co., St. Louis, MO, USA and were used for the supplementation of RPMI-1640 medium prior to use. 0.025% (*w/v*) Trypsin (Sigma Chemical Co., St. Louis, MO, USA) was used for the harvesting of cells. 1% (*v/v*) Acetic acid (Sigma Chemical Co., St. Louis, MO, USA) was used for dissolving the unbound SRB dye. 0.4% Sulphorhodamine-B (SRB) (Sigma Chemical Co., St. Louis, MO, USA) dissolved in 1% acetic acid was used as a protein dye. A stock solution of trichloroacetic acid (TCA, 50%, Sigma Chemical Co., St. Louis, MO, USA) was prepared and stored. 50 μl of the stock was added to 200 μl RPMI-1640 medium/well to yield a final concentration of 10% used for protein precipitation. 100% Isopropanol and 70% ethanol were used. Tris base 10 mM (pH 10.5) was used for SRB dye solubilization. 121.1 g of tris base was dissolved in 1000 ml of distilled water and pH was adjusted by HCl acid (2 M).

2.3 | Measurements

Microanalyses of carbon, hydrogen and nitrogen were carried out at the microanalytical Center, Cairo University, Egypt, using CHNS-932 (LECO) Vario Elemental Analyzer. Analyses of the metals followed the dissolution of the solid complex in concentrated HNO_3 , neutralizing the diluted aqueous solutions with ammonia and titrating the metal solutions with EDTA. FT-IR spectra were recorded on a Perkin-Elmer 1650 spectrometer (4000–400 cm^{-1}) in KBr discs. Electronic spectra were recorded at room temperature on a Shimadzu 3101pc spectrophotometer as solutions in DMF. ^1H NMR spectra, as a solution in $\text{DMSO}-d_6$, were recorded on a 300 MHz Varian-Oxford Mercury at room temperature using TMS as an internal standard.

Molar conductivities of 10^{-3} M solutions of the solid complexes in DMF:DMSO (1:1) were measured using Jenway 4010 conductivity meter. UV-vis spectra were recorded at room temperature on a Shimadzu 3101pc spectrophotometer as solutions in ethanol. The thermogravimetric analyses (TG and DTG) of the solid complexes were carried out from room temperature to 1000 $^{\circ}\text{C}$ using a Shimadzu TG-

50H thermal analyzer. The anticancer activity was performed at the National Cancer Institute, Cancer Biology Department, Pharmacology Department, Cairo University. The optical density (O.D.) of each well was measured spectrophotometrically at 564 nm with an ELIZA microplate reader (Meter tech. Σ 960, USA). The molecular structure of the investigated ligand was optimized by DFT based B3LYP method along with the LANL2DZ basis set. The molecule was built with the Perkin Elmer ChemBio Draw and optimized using Perkin Elmer ChemBio3D software.^[14,15] The biological activity was carried out in the regional center for mycology and biotechnology, Al-Azhar University.

2.4 | Preparation of acetyl ferrocene Schiff base ligand HL

The new Schiff base ligand was prepared by mixing equal amounts of hot saturated ethanolic solution of the acetyl ferrocene (8 g, mmol) and 2-aminobenzoic acid (anthranilic acid, 4.8 g, mmol). The mixture was refluxed for three hours. The resulting ligand was filtered and washed several times with hot ethanol until the filtrates become clear. The solid ligand then dried in desiccator over anhydrous calcium chloride. The yield was 72%.

Yield 97%; dark brown solid, *m.p.* > 300 $^{\circ}\text{C}$. Anal. Calcd. for $\text{C}_{19}\text{H}_{17}\text{FeNO}_2$ (%): C, 65.71; H, 4.90; N, 4.03; Fe, 16.14. Found (%): C, 65.40; H, 4.46; N, 3.74; Fe, 16.04. IR (ν , cm^{-1}): 3426br (OH), 1780 m (C=O), 1615s (C=N), 1590sh (COO)_{asym}, 1403sh (COO)_{sym}, 1158 m (C-N). UV-vis (λ_{max} , nm): 268 (π - π^*), 328 (n - π^*). The ^1H NMR: 11.41 ppm (s, 1H, COOH), 6.47–7.98 ppm (m, 4H, benzene ring) and 4.23–4.77 (m, 9H, ferrocene rings).

2.5 | Preparation of metal complexes

The present metal complexes were prepared by mixing equal amounts of hot saturated ethanolic solution of the Schiff base ligand (HL; 0.008 mol) with the same ratio of metal chloride (1 M:1HL molar ratio). The mixture was refluxed for three hours. The resulting complexes were filtered and washed several times with hot ethanol until the filtrates become clear. The solid complexes then dried in desiccator over anhydrous calcium chloride. The yield ranged from 66–99%.

$[\text{Cr}(\text{L})(\text{Cl})(\text{H}_2\text{O})_3]\text{Cl}\cdot 2\text{H}_2\text{O}$

Yield 87%; dark brown solid, *m.p.* 252 $^{\circ}\text{C}$. Anal. Calcd. for $\text{Cr}(\text{C}_{19}\text{H}_{26}\text{Cl}_2\text{FeNO}_7)$ (%): C, 40.79; H, 4.65; N, 2.50; Cl, 12.70; Cr, 9.30. Found (%): C, 40.63; H, 4.26; N, 2.31; Cl, 12.33; Cr, 8.86. IR (ν , cm^{-1}): 3426br (OH), disappear (C=O), 1648sh (C=N), 1600s (COO)_{asym}, 1425 m (COO)_{sym}, 1161 m (C-N), 940 s and 871 m (H_2O coordinated water), 582 s (M-O), 541 s (M-O coordinated water), 483 s (M-N). UV-vis (λ_{max} , nm): 269 (π - π^*), 391 (n - π^*).

[Mn(L)(Cl)(H₂O)₃].H₂O

Yield 57%; Dark brown solid, m.p 246°C. Anal. Calcd. for Mn(C₁₉H₂₄ClFeNO₆) (%):C, 44.84; H, 4.72; N, 2.75; Cl, 6.98; Mn, 10.82. Found (%): C, 44.62; H, 4.62; N, 2.33; Cl, 6.50; Mn, 10.78. IR (ν , cm⁻¹): 3424br (OH), disappear (C=O), 1623 m (C=N), disappear (COO)_{asym}, 1428 m (COO)_{sym}, 1164 m (C-N), 933 s and 877 m (H₂O coordinated water), 596 s (M-O), 543 s (M-O coordinated water), 485 s (M-N). Uv-vis (λ_{max} , nm): 289 (π - π^*), 318 (n- π^*).

[Fe(L)(Cl)(H₂O)₃].Cl.H₂O

Yield 69%; dark brown solid, m.p 184°C. Anal. Calcd. for Fe(C₁₉H₂₄Cl₂FeNO₆) (%):C, 41.83; H, 4.40; N, 2.57; Cl, 13.03; Fe, 10.28. Found (%): C, 41.69; H, 4.32; N, 2.48; Cl, 12.94; Fe, 10.07. IR (ν , cm⁻¹): 3420br (OH), 1720s (C=O), 1634sh (C=N), 1580s (COO)_{asym}, 1429sh (COO)_{sym}, 1180 m (C-N), 951 s and 852 m (H₂O coordinated water), 591 s (M-O), 545 s (M-O coordinated water), 487 s (M-N). Uv-vis (λ_{max} , nm): 275 (π - π^*), 314 (n- π^*).

[Co(L)(Cl)(H₂O)₃].H₂O

Yield 66%; dark brown solid, m.p > 218°C. Anal. Calcd. for Co(C₁₉H₂₄ClFeNO₆) (%):C, 44.48; H, 4.68; N, 2.73; Cl, 6.93; Co, 11.51. Found (%): C, 44.28; H, 4.52; N, 2.42; Cl, 6.80; Co, 11.93. IR (ν , cm⁻¹): 3424br (OH), disappear (C=O), 1626 m (C=N), 1560s (COO)_{asym}, 1428 m (COO)_{sym}, 1160 m (C-N), 935 s and 875 m (H₂O of coordinated water), 586 s (M-O), 537 s (M-O coordinated water), 482 s (M-N). Uv-vis (λ_{max} , nm): 268 (π - π^*), 381 (n- π^*).

[Ni(L)(Cl)(H₂O)₃]

Yield 99%; dark brown solid, m.p 94°C. Anal. Calcd. for Ni(C₁₉H₂₂ClFeNO₅) (%):C, 46.11; H, 4.45; N, 2.83; Cl, 7.18; Ni, 11.93. Found (%): C, 45.88; H, 4.32; N, 2.63; Cl, 7.02; Ni, 11.81. IR (ν , cm⁻¹): 3309br (OH), 1820s (C=O), 1652sh (C=N), 1581s (COO)_{asym}, 1435s (COO)_{sym}, 1157 m (C-N), 950 s and 872 m (H₂O coordinated water), 599 s (M-O), 540 s (M-O coordinated water), 493 s (M-N). Uv-vis (λ_{max} , nm): 275 (π - π^*), 350 (n- π^*).

[Cu(L)(Cl)(H₂O)₃]

Yield 57%; dark green solid, m.p 224°C. Anal. Calcd. for Cu(C₁₉H₂₂ClFeNO₅) (%):C, 45.69; H, 4.41; N, 2.81; Cl, 7.11; Cu, 12.73. Found (%): C, 45.36; H, 4.30; N, 2.91; Cl, 6.88; Cu, 12.54. IR (ν , cm⁻¹): 3410br (OH), 1722s (C=O), 1615s (C=N), 1560s (COO)_{asym}, 1436 m (COO)_{sym}, 1183s (C-N), 952 s and 876 m (H₂O coordinated water), 582 s (M-O), 555 s (M-O coordinated water), 473 s (M-N). Uv-vis (λ_{max} , nm): 273 (π - π^*), 321 (n- π^*).

[Zn(L)(Cl)(H₂O)₃].2H₂O

Yield 69%; dark brown solid, m.p 140°C. Anal. Calcd. for Zn(C₁₉H₂₆ClFeNO₇) (%):C, 42.50; H, 4.85; N, 2.61; Cl,

6.62; Zn, 12.12. Found (%): C, 42.40; H, 4.69; N, 2.16; Cl, 6.60; Zn, 11.97. IR (ν , cm⁻¹): 3442br (OH), disappear (C=O), 1654sh (C=N), 1590s (COO)_{asym}, 1435s (COO)_{sym}, 1162s (C-N), 945 s and 877 m (H₂O coordinated water), 568 s (M-O), 547 s (M-O coordinated water), 473 s (M-N). Uv-vis (λ_{max} , nm): 271 (π - π^*), disappear (n- π^*).

[Cd(L)(Cl)(H₂O)₃].3H₂O

Yield 38%; dark brown solid, m.p 180°C. Anal. Calcd. for Cd(C₁₉H₂₈ClFeNO₈) (%):C, 37.91; H, 4.66; N, 2.33; Cl, 5.90; Cd, 18.62. Found (%): C, 37.69; H, 4.42; N, 2.15; Cl, 5.61; Cd, 18.41. IR (ν , cm⁻¹): 3449br (OH), disappear (C=O), 1615s (C=N), 1583s (COO)_{asym}, 1448s (COO)_{sym}, 1191s (C-N), 935 s and 876 m (H₂O coordinated water), 591 s (M-O), 537 s (M-O coordinated water), 481 s (M-N). Uv-vis (λ_{max} , nm): 276 (π - π^*), disappear (n- π^*).

2.6 | Spectrophotometric studies

The absorption spectra of HL ligand and its metal complexes under study were scanned within the wavelength range from 200 to 700 nm.

2.7 | Antimicrobial activity

The in vitro antibacterial and antifungal activity tests were performed through the disc diffusion method^[16] using getamicin as positive control for Gram(+) bacteria, ampicillin for Gram(-) bacteria and amphotericin for the four fungi, respectively. The bacterial organisms used are Gram (+) bacteria: *Streptococcus pneumoniae* and *Bacillus subtilis*, Gram (-) bacteria: *Pseudomonas aeruginosa* and *Escherichia coli* and fungi like: *Aspergillus fumigatu*, *Syncephalastrum racemosum*, *Geotricum candidum* and *Candida albicans*. Stock solution (0.001 mol) was prepared by dissolving the compounds in DMSO. The nutrient agar medium for antibacterial was (0.5% Peptone, 0.1% Beef extract, 0.2% Yeast extract, 0.5% NaCl and 1.5% Agar-Agar) was prepared and then cooled to 47°C and seeded with tested microorganisms. After solidification 5 mm diameter holes were punched by a sterile corkborer. The investigated compounds, i.e. ligand and their complexes, were introduced in Petri-dishes (only 0.1 m) after dissolving in DMSO at 1.0x10⁻³ M. These culture plates were then incubated at 37°C for 20 h for bacteria. The activity was determined by measuring the diameter of the inhibition zone (in mm). The plates were kept for incubation at 37°C for 24 h and then the plates were examined for the formation of zone of inhibition. The diameter of the inhibition zone was measured in millimeters. Antimicrobial activities were performed in triplicate and the average was taken as the final reading.^[17]

2.8 | Anticancer activity

Potential cytotoxicity of the compounds was tested using the method of Skehan and Storeng.^[18] Cells were plated in 96-multiwell plate (104 cells/well) for 24 h before treatment with the compounds to allow attachment of cell to the wall of the plate. Different concentrations of the compounds under investigation (0, 5, 12.5, 25, 50 and 100 µg/ml) were added to the cell monolayer and triplicate wells were prepared for each individual dose. The monolayer cells were incubated with the compounds for 48 h at 37°C and in 5% CO₂ atmosphere. After 48 h, cells were fixed, washed and stained with SRB stain. Excess stain was washed with acetic acid and attached stain was recovered with tris-EDTA buffer. The optical density (O.D.) of each well was measured spectrophotometrically at 564 nm with an ELIZA microplate reader and the mean background absorbance was automatically subtracted and mean values of each drug concentration was calculated. The relation between surviving fraction and drug concentration is plotted to get the survival curve of breast tumor cell line for each compound.

Calculation:

The percentage of cell survival was calculated as follows:
Survival fraction = O.D. (treated cells)/ O.D. (control cells).

The IC₅₀ values (the concentrations of the HL ligand or complexes required to produce 50% inhibition of cell growth). The experiment was repeated 3 times.

2.9 | Computational methodology

The electronic structure calculation of HL ligand was carried out using the Gaussian03 suite of program.^[19] They were fully optimized employing DFT based B3LYP method along with the LANL2DZ basis set. In order to incorporate the effect of the solvent around the molecule, the TD-DFT method (along with LANL2DZ basic set) was used to calculate the electronic absorption spectra of the ligand. The contribution of molecular orbital on HOMO and LUMO were also calculated.

2.10 | Molecular docking

In order to find out the possible binding modes of the most active compounds against DNA of human-DNA-Topo I complex (1SC7), the receptors of breast cancer mutant 3HB5-oxidoreductase (3HB5), crystal structure of *Escherichia coli* (3 T88) molecular docking studies were performed using MOE 2008 software and it is a rigid molecular docking software.^[20] Docking is an interactive molecular graphics program for calculating and displaying feasible docking modes of a receptor and ligand and complex molecules. It necessitates the ligand and the receptor as input in PDB format. The amino acid chain was kept and the water molecules and

co-crystallized ligands were removed. The structure of ligand in PDB file format was created by Gaussian03 software. The crystal structures of the human-DNA-Topo I complex (PDB ID: 1SC7), the receptors of breast cancer mutant 3HB5-oxidoreductase (PDB ID: 3HB5) and crystal structure of *Escherichia coli* (PDB ID: 3 T88) were downloaded from the protein data bank (<http://www.rcsb.org/pdb>).

3 | RESULTS AND DISCUSSION

3.1 | Characterization of Schiff base ligand

The dark brown Schiff base ligand (HL) obtained by the condensation reaction between 2-acetyl ferrocene and anthranilic acid in hot ethanolic solution as a solvent, was stable in air and soluble in the most common organic solvents. The data of C, H and N content of HL referred to a molecular formula of C₁₉H₁₇FeNO₂ were shown in the experimental part.

These data were found to be in good accordance with the calculated value based on the synthetic and proposed structure. Formation of the new ligand was evidenced by the presence of a strong IR band at 1615 cm⁻¹ due to ν(C=N), while no bands attributable to ν(C=O) of acetyl ferrocene or ν(NH₂) of anthranilic acid have been detected^[21] confirming the formation of the Schiff base ligand. The ¹H NMR spectrum was recorded for HL. The proton of carboxylic group appeared as singlet at 11.41 ppm while the aromatic protons appeared as a set of multiplet in the region 6.47–7.98 ppm. The spectrum also revealed signals at 4.23–4.77 ppm (m, 9H, ferrocene rings), which can assigned to the cyclopentadiene aromatic ferrocene protons.

The electronic emission spectral data of HL was recorded in 10⁻⁴ M DMF solution. The electronic absorption spectrum of HL gave first sharp band at 268 nm which is mainly attributed to the locally excited intraligand π → π* transitions. The second band observed at 328 nm can be attributed to n-π* electronic transition.^[22]

The structure of the Schiff base ligand was confirmed by carrying out mass spectral analysis. The spectrum showed a peak at 346.87 amu (M-1) corresponding to the molecular ion peak of the ligand moiety [(C₁₉H₁₇FeNO₂), atomic mass 347.21 amu]. The observed peak was in good agreement with the proposed formula as indicated by the microanalytical data.

Thermogravimetric (TG) curve for HL ligand of the formula [C₁₉H₁₇FeNO₂] showed four weight loss events. The first and second steps of decomposition occurred within the range of 46–363°C, with two maximum temperatures at 136 and 315 °C, correspond to the loss of C₇H₁₀N fragment with estimated mass loss of 30.94% (calculated mass loss =31.12%). The third and fourth steps of decomposition occurred within the range of 364–480°C with maximum temperatures at 370 and 405.5°C which correspond to loss of

C₁₀H₇O fragment with estimated mass loss of 39.89% (calculated mass loss = 41.21%) leaving metal oxide FeO contaminated with two carbon atoms as a residue. The overall weight loss amounted to 72.83% (calculated mass loss = 72.33%).

3.1.1 | Geometrical optimization of the ligand

The selected geometrical structure of the investigated ligand (HL) is calculated by optimizing their bond lengths and bond angles presented in Table 1. Both the highest occupied molecular orbital (HOMO) and lowest unoccupied molecular orbital (LUMO) are the main orbital takes part in chemical stability. The HOMO represents the ability to donate an electron, LUMO as an electron acceptor represents the ability to obtain an electron. The HOMO and LUMO for ligand (HL) are shown in Figure 2. The calculated quantum chemical parameters are given in Table 2. Additional parameters such as ΔE , absolute electronegativities, χ , chemical potentials, P_i , absolute hardness, η , absolute softness, σ , global electrophilicity, ω , global softness, S and additional electronic charge, ΔN_{\max} have been calculated according to the following equations (1–8) [13–15]:

$$\Delta E = E_{LUMO} - E_{HOMO} \quad (1)$$

$$\chi = \frac{-(E_{HOMO} + E_{LUMO})}{2} \quad (2)$$

$$\eta = \frac{E_{LUMO} - E_{HOMO}}{2} \quad (3)$$

$$\sigma = \frac{1}{\eta} \quad (4)$$

$$P_i = -\chi \quad (5)$$

$$S = \frac{1}{2\eta} \quad (6)$$

$$\omega = \frac{P_i^2}{2\eta} \quad (7)$$

$$\Delta N_{\max} = -\frac{P_i}{\eta} \quad (8)$$

The HOMO–LUMO energy gap, ΔE , which is an important stability index, is applied to develop theoretical models for explaining the structure and conformation barriers in many molecular. [23,24]

The data calculated were presented in Tables 1, 2 and reflected the following notes:

TABLE 1 The different optimized parameters of HL ligand

Bond lengths (Å)	HL
Fe(1)-C(2)	2.1269
Fe(1)-C(3)	2.1261
Fe(1)-C(4)	2.12
Fe(1)-C(5)	2.1178
Fe(1)-C(6)	2.1203
Fe(1)-C(12)	2.1211
Fe(1)-C(13)	2.1309
Fe(1)-C(14)	2.1271
Fe(1)-C(15)	2.1275
Fe(1)-C(16)	2.1067
C(2)-C(3)	1.4427
C(2)-C(6)	1.443
C(2)-H(7)	1.0814
C(3)-C(4)	1.4428
C(3)-H(8)	1.081
C(4)-C(5)	1.4423
C(4)-H(9)	1.0811
C(5)-C(6)	1.4431
C(5)-H(10)	1.0811
C(6)-H(11)	1.081
C(12)-C(13)	1.4422
C(12)-C(16)	1.4341
C(12)-H(17)	1.0808
C(13)-C(14)	1.4348
C(13)-H(18)	1.081
C(14)-C(15)	1.4561
C(14)-H(19)	1.0774
C(15)-C(16)	1.4577
C(15)-C(21)	1.4847
C(16)-H(20)	1.0798
C(21)-C(22)	1.5236
C(21)-N(26)	1.3055
C(22)-H(23)	1.0919
C(22)-H(24)	1.0981
C(22)-H(25)	1.0985
N(26)-C(32)	1.4144
C(27)-C(28)	1.4063
C(27)-C(32)	1.4122
C(27)-H(33)	1.0847
C(28)-C(29)	1.4107
C(28)-H(34)	1.0873

(Continues)

TABLE 1 (Continued)

Bond lengths (Å)	HL
C(29)-C(30)	1.407
C(29)-H(35)	1.0872
C(30)-C(31)	1.402
C(30)-H(36)	1.0857
C(31)-C(32)	1.4264
C(31)-C(37)	1.3884
C(37)-O(38)	0.9901
Bond angles (°)	
C(2)-Fe(1)-C(4)	66.6933
C(2)-Fe(1)-C(5)	66.7335
C(2)-Fe(1)-C(12)	161.3366
C(2)-Fe(1)-C(13)	158.4536
C(2)-Fe(1)-C(14)	124.9998
C(2)-Fe(1)-C(15)	111.0924
C(2)-Fe(1)-C(16)	126.8877
C(3)-Fe(1)-C(5)	66.7325
C(3)-Fe(1)-C(6)	66.699
C(3)-Fe(1)-C(12)	156.1993
C(3)-Fe(1)-C(13)	123.0805
C(3)-Fe(1)-C(14)	110.9152
C(3)-Fe(1)-C(15)	127.3711
C(3)-Fe(1)-C(16)	163.4291
C(4)-Fe(1)-C(6)	66.8095
C(4)-Fe(1)-C(12)	120.7715
C(4)-Fe(1)-C(13)	108.3752
C(4)-Fe(1)-C(14)	125.6812
C(4)-Fe(1)-C(15)	162.4942
C(4)-Fe(1)-C(16)	155.2384
C(5)-Fe(1)-C(12)	107.1205
C(5)-Fe(1)-C(14)	160.2748
C(5)-Fe(1)-C(15)	157.0284
C(5)-Fe(1)-C(16)	121.1491
C(6)-Fe(1)-C(12)	124.3546
C(6)-Fe(1)-C(13)	159.8685
C(6)-Fe(1)-C(14)	159.1674
C(6)-Fe(1)-C(15)	123.5363
C(6)-Fe(1)-C(16)	109.0634
C(12)-Fe(1)-C(14)	66.6185
C(12)-Fe(1)-C(15)	67.2027
C(13)-Fe(1)-C(15)	66.8672

(Continues)

TABLE 1 (Continued)

Bond lengths (Å)	HL
C(13)-Fe(1)-C(16)	66.5511
C(14)-Fe(1)-C(16)	66.9176
Fe(1)-C(2)-H(7)	125.4162
C(3)-C(2)-C(6)	107.9933
A(3)-C(2)-H(7)	126.0891
A(6)-C(2)-H(7)	125.9173
Fe(1)-C(3)-H(8)	125.839
C(2)-C(3)-C(4)	108.0092
C(2)-C(3)-H(8)	126.2502
C(4)-C(3)-H(8)	125.739
Fe(1)-C(4)-H(9)	124.8744
C(3)-C(4)-C(5)	108.0038
C(3)-C(4)-H(9)	125.9762
C(5)-C(4)-H(9)	126.0186
Fe(1)-C(5)-H(10)	124.6237
C(4)-C(5)-C(6)	108.0114
C(4)-C(5)-H(HH10)	125.9678
C(6)-C(5)-H(10)	126.0162
Fe(1)-C(6)-H(11)	125.4437
C(2)-C(6)-C(5)	107.9821
C(2)-C(6)-H(11)	126.0472
C(5)-C(6)-H(11)	125.9699
Fe(1)-C(12)-H(17)	124.9559
C(13)-C(12)-C(16)	107.8712
C(13)-C(12)-H(17)	126.1913
C(16)-C(12)-H(17)	125.9356
Fe(1)-C(13)-H(18)	125.3493
C(12)-C(13)-C(14)	108.3615
C(12)-C(13)-H(18)	126.0731
C(14)-C(13)-H(18)	125.563
Fe(1)-C(14)-H(19)	126.371
C(13)-C(14)-C(15)	108.5005
C(13)-C(14)-H(19)	125.3065
C(15)-C(14)-H(19)	126.1808
Fe(1)-C(15)-C(21)	130.2923
C(14)-C(15)-C(16)	106.4758
C(14)-C(15)-C(21)	130.0137
C(16)-C(15)-C(21)	123.2258
Fe(1)-C(16)-C(20)	125.2519
C(12)-C(16)-C(15)	108.7893

(Continues)

TABLE 1 (Continued)

Bond lengths (Å)	HL
C(12)-C(16)-C(20)	125.3362
C(15)-C(16)-C(20)	125.87
C(15)-C(21)-C(22)	115.532
C(15)-C(21)-C(26)	129.0757
C(22)-C(21)-C(26)	115.2421
C(21)-C(22)-H(23)	109.1395
C(21)-C(22)-H(24)	111.3258
C(21)-C(22)-H(25)	110.8814
H(23)-C(22)-H(24)	109.2108
H(23)-C(22)-H(25)	108.7208
H(24)-C(22)-H(25)	107.5059
C(21)-N(26)-C(32)	131.4356
C(28)-C(27)-C(32)	120.4547
C(28)-C(27)-C(33)	120.163
C(32)-C(27)-H(33)	119.3733
C(27)-C(28)-C(29)	120.1853
C(27)-C(28)-H(34)	119.757
C(29)-C(28)-H(34)	120.0572
C(28)-C(29)-C(30)	120.2606
C(28)-C(29)-H(35)	120.1174
C(30)-C(29)-H(35)	119.6125
C(29)-C(30)-C(31)	119.3279
C(29)-C(30)-H(36)	121.7292
C(31)-C(30)-H(36)	118.9309
C(30)-C(31)-C(32)	121.2402
C(30)-C(31)-C(37)	119.8272
C(32)-C(31)-C(37)	118.9326
N(26)-C(32)-C(27)	127.1277
N(26)-C(32)-C(31)	113.722
C(27)-C(32)-C(31)	118.4141
C(31)-C(37)-O(38)	107.1679

i The data of HL had a great chance and priority for biological activity based on high ω value.

ii S and ω were the softness indexes while η is for hardness indication; a hard molecule had a high stability due to its high energy difference in-between the E_{HOMO} and E_{LUMO} than the soft molecule. So, the soft molecule was the reactive one having flexible donation towards the metal ions. Accordingly, the investigated HL molecule was soft towards the coordination.

iii The positive electrophilicity index (χ) value and the negative chemical potential (Pi) value indicated that the HL

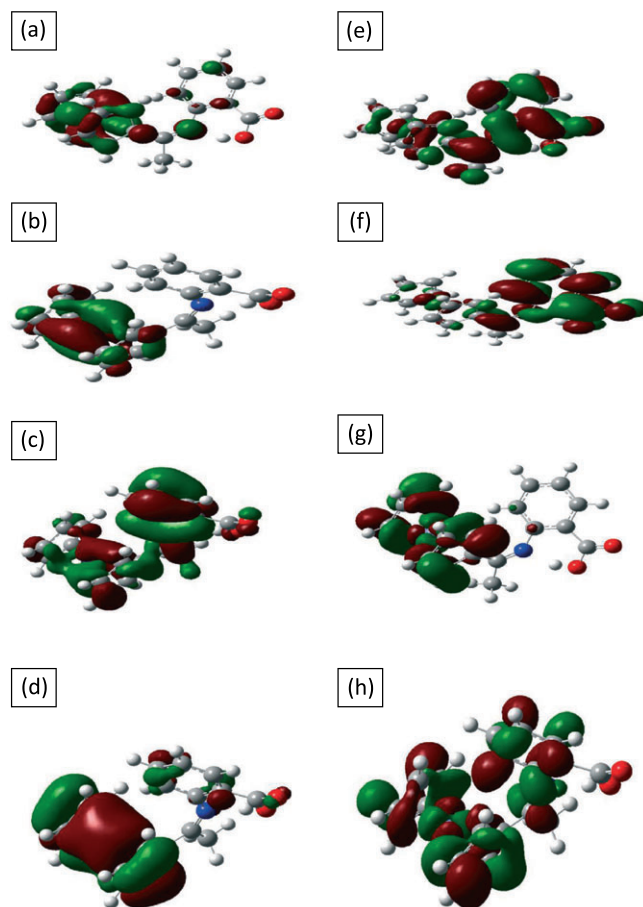


FIGURE 2 The different molecular orbitals of ligand (HL), (a) HOMO, (b) HOMO-1, (c) HOMO-2, (d) HOMO-3, (e) LUMO, (f) LUMO + 1, (g) LUMO + 2 and (h) LUMO + 3

TABLE 2 The different quantum chemical parameters of HL ligand

The calculated quantum chemical parameters	
E (a.u.)	-1062.74
Dipole moment (Debye)	10.15
E_{HOMO} (eV)	-0.221
E_{LUMO} (eV)	-0.081
ΔE (eV)	0.139
χ (eV)	0.151
η (eV)	0.0695
σ (eV) ⁻¹	14.38
Pi (eV)	-0.151
S (eV) ⁻¹	7.194
ω (eV)	0.164
ΔN_{max}	2.171

molecule capable of accepting electrons from the environment and its energy must decrease upon accepting electronic charge. Therefore, the electronic chemical potential must be negative.^[25]

- iv The total energy of free ligand was small, which indicated greatly the stability of the isolated Schiff base ligand.
- v The small energy gap can be associated with a high chemical reactivity, low kinetic stability and reflects to efficient electronic charge transfer interaction making the molecule highly polarizable.

3.1.2 | Molecular electrostatic potential (MEP)

The MEP is a plot of electrostatic potential mapped onto the constant electron density surface. It is also very useful in research of molecular structure with its physiochemical property relationship as well as hydrogen bonding interactions.^[26–28] The electrostatic potential $V(r)$ at a given point r (x, y, z) is defined in terms of the interaction energy between the electrical charge generated from the molecule electrons, nuclei and proton located at r . Computation of electrostatic potential is possible for molecules using the G-point and multiple k-points. In this study, 3D plots of molecular electrostatic potential (MEP) of ligands Figure 3 has been drawn. The maximum negative region which is preferred site for electrophilic attack indications represented as red color, the maximum positive region which is preferred site for nucleophilic attack symptoms as blue color. Potential increases in the order red < green < blue, where blue shows the strongest attraction and red shows the strongest repulsion. Regions having the negative potential are over the electronegative atoms while the regions having the positive potential are over the hydrogen atoms.^[26] The MEP showed that the negative potential site was situated over carboxylate oxygen and nitrogen atom and the positive potential site were present around the hydrogen atoms. The regions over the rings were neutral

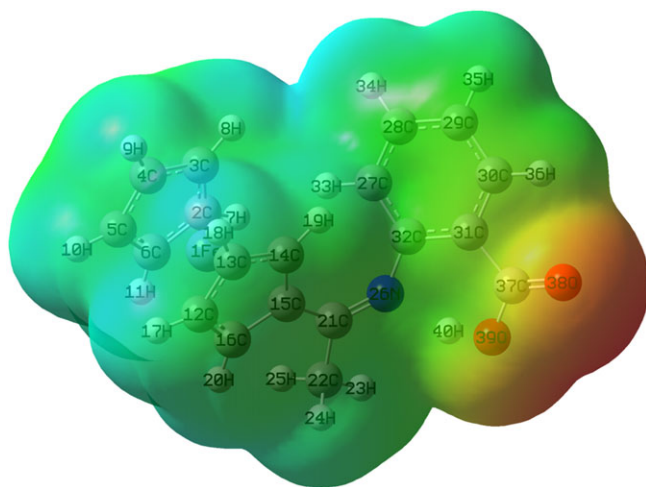


FIGURE 3 Molecular electrostatic potential map of HL ligand, The electron density isosurface is 0.004 a.u.

and it was represented by green color. These sites gave information about the regions that can be considered as a site of electrophilic attack by the metal ions during complexation process.^[29,30]

3.1.3 | Mulliken charge analyses

Mulliken atomic charges for some important atoms were calculated and the data are listed in Table 3 and shown in Figure 4. The calculation of atomic charges plays an important role in the application of quantum mechanical calculations to molecular systems.^[31] From Table 3, the calculated charge value for N and O are -0.292 and -0.282 a.u., indicates the high electronegativity around them and high probability of electron transfer from these atoms to metal center in the proposed complexes. Oxygen and nitrogen atoms in HL had more negative charges than the other atoms. The C₂₁, C₃₂ and C₃₇ atoms had higher positive atomic charges than the other carbon atoms. This was due to the electronegative atoms such as oxygen and nitrogen attached to

TABLE 3 The different Mulliken charges of HL Ligand

HL	
Atom	Mulliken charges
Fe	0.151382
C2	0.028469
C3	0.024879
C4	0.023809
C5	0.032548
C6	0.021314
C12	0.026685
C13	0.031283
C14	0.010986
C15	0.254275
C16	-0.05782
C21	0.045172
C22	-0.04979
N26	-0.29154
C27	-0.0559
C28	0.005229
C29	-0.00292
C30	-0.05411
C31	0.016685
C32	0.28217
C37	0.158256
O38	-0.28225
O39	-0.01606

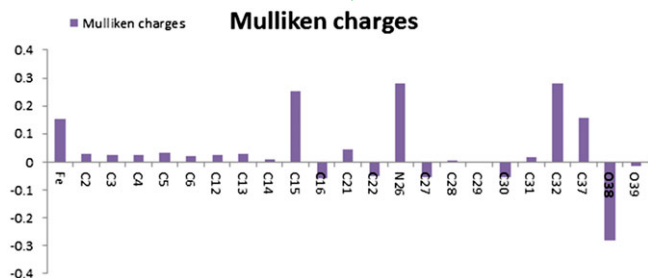


FIGURE 4 Mulliken charges for free HL ligand

carbon atoms. Mulliken method was used for predicting the suitable sites of coordination to the metal ions present in Schiff base HL ligand, which was also estimated from MEP analysis.^[29–31]

3.1.4 | Vibrational properties

Theoretical harmonic vibrational analysis has been also performed based on the optimized geometry. It was well known that the vibrational frequencies computed at quantum chemical methods such as DFT levels contain well-known systematic errors. The scaling factor of 0.96 for LanL2DZ level was used to correct the effects of anharmonicity and neglected part of electron correlation.^[32–34] The FT-IR and its theoretical corresponding spectra for HL were shown in Figure 5. The stretching vibration of a free or non-hydrogen bonded OH group appeared experimentally at 3453 cm^{-1} .^[34] The OH stretching mode of HL was calculated theoretically at 3469 cm^{-1} . The stretching vibration of C=N group was

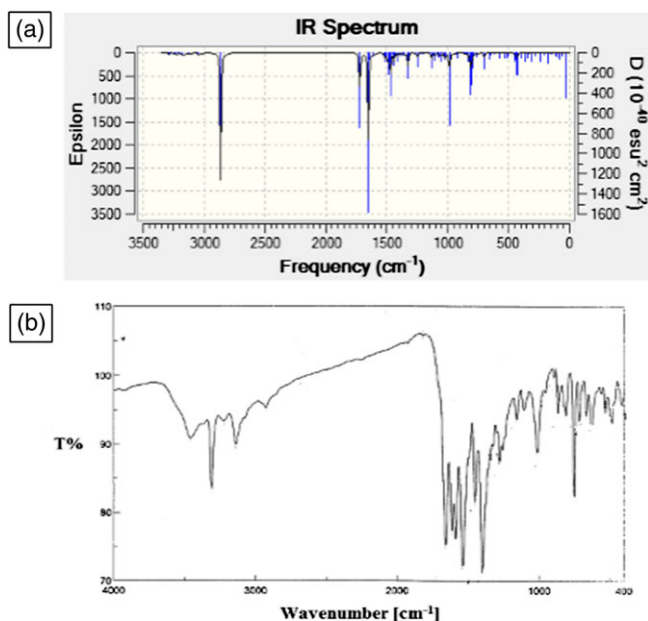


FIGURE 5 IR spectra of HL (a) theoretical spectrum, (b) experimental spectrum

found at 1615 cm^{-1} . It was noted that the calculated values were close to the theoretical data of 1650 cm^{-1} , see Figure 5.

3.2 | Characterization of ligand metal complexes

The new Schiff base ligand (HL) and its Cr(III), Mn(II), Fe(III), Co(II), Ni(II), Cu(II), Zn(II) and Cd(II) complexes were characterized using different spectroscopic techniques, elemental analyses, magnetic, solid reflectance and thermal studies.^[32] Accordingly, the structure of HL ligand is given in Figure 1.

3.2.1 | Elemental analysis

The stoichiometry and formulation of the HL (Figure 1) and its metal complexes were confirmed by their elemental analysis. The metal/ligand ratio was found to be 1:1 in all complexes, which have been arrived by estimating the carbon, hydrogen, nitrogen, chloride and metal contents of the complexes. The elemental analyses of the ligand and its complexes reveal good agreement with the proposed structures. The ligand and its metal complexes have high melting points, and they are found to be air stable. The Ligand is soluble in common organic solvents, and all the complexes are freely soluble in DMF and DMSO but insoluble in methanol, ethanol and water.^[33]

3.2.2 | Molar conductivity measurements

The metal (II) and (III) complexes were dissolved in DMF or DMF:DMSO (1:1) and molar conductivities of the solutions at room temperature were measured. The conductance data indicates that some of the metal complexes are having conductivity values in accordance with electrolytes.^[34,35]

The results given in Table 4 showed that the Cr(III) and Fe(III) complexes had molar conductivity values of 80.8 and $85.1\ \Omega^{-1}\text{ mol}^{-1}\text{ cm}^2$, respectively, which indicated the ionic nature of these complexes and hence their electrolytic nature. The molar conductivity values of Mn(II), Co(II), Ni(II), Cu(II), Zn(II) and Cd(II) chelates under investigation (Table 2) were found to be 31.6, 17.7, 22.5, 11.2, 10.1 and $6.4\ \Omega^{-1}\text{ mol}^{-1}\text{ cm}^2$, respectively. It is obvious from these data that these chelates are non-ionic in nature and hence non-electrolyte.^[36]

3.2.3 | IR spectra

The characteristic peaks of the free Schiff base ligand and its metal complexes were listed in the experimental part, where the band assignments of the guide bands (those affected by coordination) have been given. The characteristic O—H, C=O and C=N bands were observed in the IR spectrum of

TABLE 4 Thermoanalytical results (TG and DTG) of HL ligand and its metal complexes

Compound	TGA range (°C)	T _g (°C)	n*	Mass loss%		Total mass loss% Found (calcd)	Assignment	Residue
				Found	Calcd.			
HL	45–365	136, 315	2	30.94	31.12	70.83	Loss of C ₇ H ₁₀ N	FeO + 2C
	365–480	370, 405.5	2	39.89	41.21	(72.33)	Loss of C ₁₀ H ₇ O	
[Cr(L)(Cl)(H ₂ O) ₃] Cl.2H ₂ O	45–250	97, 207	2	19.1	19.40	73.96	Loss of 4H ₂ O and HCl	1/2 Cr ₂ O ₃ + FeO
	250–1000	365, 529, 1000	3	54.86	54.11	(73.51)	Loss of C ₁₉ H ₁₇ ClNO _{0.5}	
[Mn(L)(Cl)(H ₂ O) ₃]. H ₂ O	45–255	118	1	31.47	30.05	71.93	Loss of 4H ₂ O and C ₅ H ₇ N	MnO + FeO
	255–670	382, 575	2	40.34	41.74	(71.79)	Loss of C ₁₄ H ₉ Cl	
[Fe(L)(Cl)(H ₂ O) ₃].Cl. H ₂ O	45–500	92, 310	2	46.22	46.05	70.39	Loss of 3H ₂ O and C ₁₄ H ₁₅ N	1/2 Fe ₂ O ₃ + FeO + C
	501–740	616	1	24.17	23.85	(70.0)	Loss of C ₅ H ₇ Cl ₂ O _{0.5}	
[Co(L)(Cl)(H ₂ O) ₃]. H ₂ O	45–385	103, 293	2	29.99	30.21	71.91	Loss of 4H ₂ O and C ₅ H ₉ N	CoO + FeO
	385–630	519	1	41.92	41.03	(71.24)	Loss of C ₁₄ H ₇ Cl	
[Ni(L)(Cl)(H ₂ O) ₃]	45–625	118, 347	2	67.94	67.97	67.94 (67.97)	Loss of 3H ₂ O and C ₁₈ H ₁₆ ClN	NiO + FeO + C
[Cu(L)(Cl)(H ₂ O) ₃]	45–285	100, 229	2	26.56	26.65	66.91	Loss of 3H ₂ O and C ₅ H ₅ N	CuO + FeO + C
	285–575	356, 575	2	40.35	40.58	(67.23)	Loss of C ₁₃ H ₁₁ Cl	
[Zn(L)(Cl) (H ₂ O) ₃].2H ₂ O	45–520	125, 347	2	41.49	41.37	70.62	Loss of 5H ₂ O and C ₉ H ₁₀ N	ZnO + FeO
	520–915	651	1	29.14	29.46	(70.72)	Loss of C ₁₀ H ₆ Cl	
[Cd(L)(Cl) (H ₂ O) ₃].3H ₂ O	45–380	134, 329	2	28.70	28.73	66.07	Loss of 6H ₂ O and C ₄ H ₃ N	CdO + FeO
	380–565	421, 502	2	37.38	37.95	(66.68)	Loss of C ₁₅ H ₁₄ Cl	

HL ligand at 3453, 1780 and 1615 cm⁻¹, respectively. The IR spectrum of HL showed broad band of carboxylic acid at 3453 cm⁻¹ which still broad in the range of 3409–3449 cm⁻¹ in the metal ion complexes. The expected azomethene C=N appears in the ligand at 1615 cm⁻¹ and in its metal complexes in the range of 1615–1654 cm⁻¹. The absence of $\nu(\text{C}=\text{O})$ stretching vibration bands in the spectra of Cr(III), Co(II), Zn(II) and Cr(II) complexes indicates strongly the involvement of carboxylic group in the coordination process. Other characteristic strong bands appearing in the metal ion complexes around 1560–1600 cm⁻¹ and 1425–1448 cm⁻¹ were attributed to $\nu_{\text{asym}}(\text{COO}^-)$ and $\nu_{\text{sym}}(\text{COO}^-)$, respectively. The difference (≈ 135 cm⁻¹) between $\nu_{\text{asym}}(\text{COO}^-)$ and $\nu_{\text{sym}}(\text{COO}^-)$ confirms the coordination mode of the carboxylate group.^[37] The $\nu(\text{M}-\text{O})$ stretching vibration of coordinated water was appeared in the range of 537–555 cm⁻¹ in all of the complexes. New band appeared in the range of 473–493 cm⁻¹ indicates the M-N interaction. From the spectra and the chemical structure of HL ligand proposed in Figure (1), it can conclude that the Schiff base ligand could be considered as mononegative bidentate ligand and coordinated to the metal ions via deprotonated carboxylate oxygen atom and azomethene nitrogen.

3.2.4 | ¹H NMR spectra

Proof of the type of bonding of HL with the metal ions was also confirmed by recording their ¹H NMR spectra in

DMSO-d₆ and in the deuterated solvent.^[38] The ¹H NMR spectrum of HL showed a peak at 11.41 ppm which was attributed to proton of the carboxylic acid group.^[39] This peak was disappeared in the spectra of Zn(II) and Cd(II) complexes, indicating that the carboxylic group played important part in coordination. The aromatic ring protons were observed as a multiplet, in the range 6.47–7.98 ppm. The ¹H NMR spectrum of the ligand revealed signals at 4.23–4.77 ppm (m, 9H, ferrocene rings), while for Zn(II) and Cd(II) complexes the signals were at 3.34 and 3.50 ppm (m, 9H, ferrocene rings), respectively, which can assigned to the aromatic protons.^[40]

3.2.5 | UV-visible spectra of ligand and its metal complexes

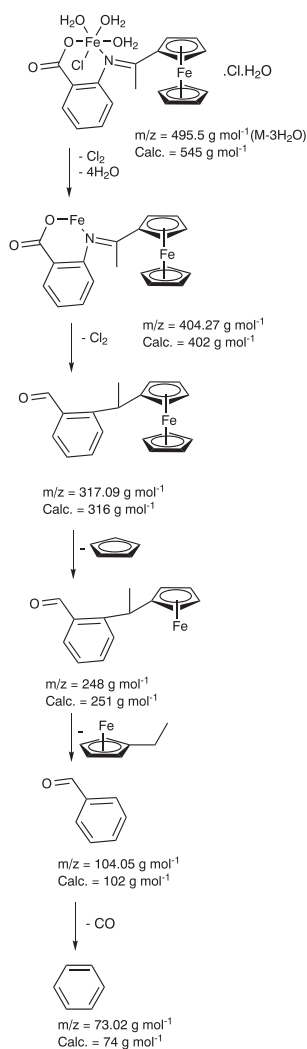
The electronic spectral data of Schiff base ligand (HL) and its transition metal complexes were recorded in 10⁻⁴ and 5 × 10⁻⁴ M DMF solution (Figure S6). The electronic absorption spectrum of HL gave sharp band at 268 nm which was mainly attributed to the locally excited intraligand $\pi \rightarrow \pi^*$ transitions.^[41] All the complexes apparently displayed a high intensity band in the 268–289 nm regions, attributable to the $\pi \rightarrow \pi^*$ intra-ligand transition and a medium intensity band in 314–381 nm regions, assigned to $n \rightarrow \pi^*$ transition.^[42] Expectedly, Co(II) and Zn(II) complexes displayed a low intensity broad band in the 537–674 nm regions attributed to the d-d transitions.^[43]

3.2.6 | Mass spectra

The iron complex also exhibited peaks at m/z 495 (calcd. = 545; $M-3H_2O$), characteristic of the $[Fe(L)(Cl)(H_2O)_3]Cl \cdot H_2O$ ^[12] (Figure S7). The molecular ion peak undergoes fragmentation and displayed multiple peaks corresponding to successive degradation of the complex (Scheme 1).^[44] The expected molecular ion peak appeared at m/z 346.87 amu in the mass spectrum of the complex assignable to the parent ion of HL ligand $[C_{19}H_{17}FeNO_2]$ in the complex.

3.2.7 | Thermal analysis of the metal complexes

The thermal behavior of all metal complexes, Cr(III), Mn(II), Fe(III), Co(II), Ni(II), Cu(II), Zn(II) and Cd(II), is generally similar. A certain difference comes from the loosing of coordinated water molecules, if it is present. Several effects were observed on the TG and DTG curves, see Table 4. The



SCHEME 1 Suggested mass fragmentation of $[Fe(L)(Cl)(H_2O)_3]Cl \cdot H_2O$ complex

theoretically calculated mass losses are in a good agreement in accordance of the observed ones. The discrepancies can be explained by the simultaneously running thermal processes.^[45]

The thermal properties of HL and its binary metal complexes were investigated using TG and DTG under nitrogen atmosphere with a heating rate of $10^\circ C \text{ min}^{-1}$ and the data obtained were listed in Table 4. It was carried out from the ambient temperature up to $1000^\circ C$ to investigate the thermal stabilities of these new metal complexes and to decide whether the water molecules (if present) were inside or outside the inner coordination sphere of the central metal ion.^[46,47]

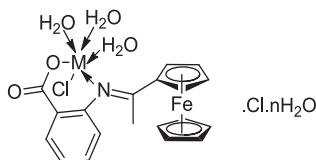
The thermogram of $[Cr(L)(Cl)(H_2O)_3]Cl \cdot 2H_2O$ complex showed five decomposition steps within the temperature range of $45\text{--}1000^\circ C$. The first and second decomposition steps accompanied by loss of two uncoordinated water, two coordinated water and HCl molecules in the temperature range of $45\text{--}250^\circ C$ with an estimated weight loss of 19.10% (calcd. 19.40%). The three final stages of decomposition showed loss of $C_{19}H_{17}ClNO_{0.5}$ molecule at $250\text{--}1000^\circ C$ with an estimated weight loss of 54.86% (calcd. 54.11%). Thereafter the percentage of the residue corresponds to chromium oxide contaminated with iron(II) oxide and the total estimated weight loss is found to be 73.96% (calcd. 73.51%).^[48,49] TG curve of the $[Mn(L)(Cl)(H_2O)_3] \cdot H_2O$ complex showed three steps of decomposition. The first stage of decomposition occurred in the $45\text{--}255^\circ C$ temperature range and corresponds to the loss of one uncoordinated water, three coordinated water and C_5H_7N molecules. It is accompanied by a weight loss of 31.47% (calcd. 30.05%). The second and third stages of decomposition involve the removal of $C_{14}H_9Cl$ molecule in the $479\text{--}668^\circ C$ temperature range, and were accompanied by a weight loss of 40.34% (calcd. 41.74%). The total weight loss amounts to 71.93% (calcd. 71.79%) leaving manganese oxide as a residue contaminated with iron(II) oxide. The thermogram of $[Fe(L)(Cl)(H_2O)_3]Cl \cdot H_2O$ complex loses weight equal to 46.22% (calcd. 46.05%) in the temperature range of $45\text{--}500^\circ C$. This corresponds to loss of three water molecules and $C_{14}H_{15}N$ molecule in the first two stages of decomposition. In the third stage, the complex shows removal of $C_5H_7Cl_2O_{0.5}$ molecule at $500\text{--}740^\circ C$ with an estimated weight loss of 24.17% (calcd. 23.85%). The total weight loss amounts to 70.39% (calcd. 70.0%) leaving ferrous and ferric oxide as a residue contaminated with carbon. The thermogram of $[Co(L)(Cl)(H_2O)_3] \cdot H_2O$ complex loses weight equal to 29.99% (calcd. 30.21%) in the temperature range of $45\text{--}385^\circ C$. This corresponds to loss of one uncoordinated water, three coordinated water and C_5H_9N molecule in the first and second stages of decomposition. In the third stage, the complex showed removal of $C_{14}H_7Cl$ molecule at $385\text{--}630^\circ C$ with a practical weight loss of 41.92% (calcd. 41.03%). The total weight loss amounts to 71.91% (calcd. 71.24%) leaving cobalt oxide as a

residue contaminated with iron(II) oxide. For $[\text{Ni}(\text{L})(\text{Cl})(\text{H}_2\text{O})_3]$ complex, it decomposed in two steps of decomposition associated with the removal of three coordinated water and $\text{C}_{18}\text{H}_{16}\text{ClN}$ molecules in the temperature range of 45–625°C. The estimated total weight loss of 67.94% (calcd. 67.91%) leaving nickel oxide as a residue contaminated with iron(II) oxide. TG curve of the $[\text{Cu}(\text{L})(\text{Cl})(\text{H}_2\text{O})_3]$ complex showed four steps of decomposition. The first and second

stages of decomposition occurred in the 45–285°C temperature range, corresponding to the loss of three coordinated and $\text{C}_5\text{H}_5\text{N}$ molecule, and is accompanied by a weight loss of 26.56% (calcd. 26.65%). The third and fourth stages of decomposition involved the removal of $\text{C}_{13}\text{H}_{11}\text{Cl}$ molecule in the 285–575°C temperature range, and are accompanied by a weight loss of 40.35% (calcd. 40.58%). The total weight loss amounts to 66.91% (calcd. 67.23%) leaving copper oxide contaminated with ferrous oxide as final residue.

TG curve of the $[\text{Zn}(\text{L})(\text{Cl})(\text{H}_2\text{O})_3] \cdot 2\text{H}_2\text{O}$ complex showed three steps of decomposition. The first and second steps of decomposition occurred in the temperature range of 45–520°C are associated with the loss of two uncoordinated water, three coordinated water and $\text{C}_9\text{H}_{10}\text{N}$ molecules with an estimated weight loss of 41.49% (calcd. 41.37%). The third step of decomposition occurs in the temperature range of 520–915°C is associated with the loss of $\text{C}_{10}\text{H}_6\text{Cl}$ molecule and with an estimated weight loss of 29.14% (calcd. 30.10%). Thereafter the weight of the residue corresponds to zinc oxide contaminated with ferrous oxide as a residue and the total estimated weight loss of 70.62% (calcd. 71.47%). TG curve of the $[\text{Cd}(\text{L})(\text{Cl})(\text{H}_2\text{O})_3] \cdot 3\text{H}_2\text{O}$ complex showed four steps of decomposition. The first and second steps of decomposition occurred in the temperature range of 45–380°C and are associated with the loss of three hydrated water, three uncoordinated water and $\text{C}_4\text{H}_3\text{N}$ molecules with an estimated weight loss of 28.70% (calcd. 28.73%). The third and fourth steps of decomposition occurred in the temperature range of 380–565°C and are associated with the loss of $\text{C}_{15}\text{H}_{13}\text{Cl}$ molecule and with an

(a) In case of Cr(III) and Fe(III) complexes (where $n = 4$ for Er(III) and Yb(III) complexes, $n = 3$ for La(III) complex, $n = 2$ for Cr(III) complex and $n = 1$ for Fe(III) complex)



(b) In case of Mn(II), Co(II), Ni(II), Cu(II), Zn(II) and Cd(II) complexes (where $n = 3$ for Cd(II) complex, $n = 2$ for Zn(II) complex, $n = 1$ for Mn(II) and Co(II), and $n = 0$ for Ni(II) and Cu(II))

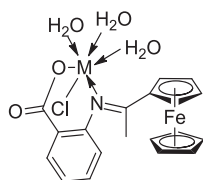


FIGURE 6 The structure of metal complexes. a) In case of Cr(III) and Fe(III) complexes (where $n = 2$ for Cr(III) complex and $n = 1$ for Fe(III) complex). b) In case of Mn(II), Co(II), Ni(II), Cu(II), Zn(II) and Cd(II) complexes (where $n = 3$ for Cd(II) complex, $n = 2$ for Zn(II) complex, $n = 1$ for Mn(II) and Co(II), and $n = 0$ for Ni(II) and Cu(II))

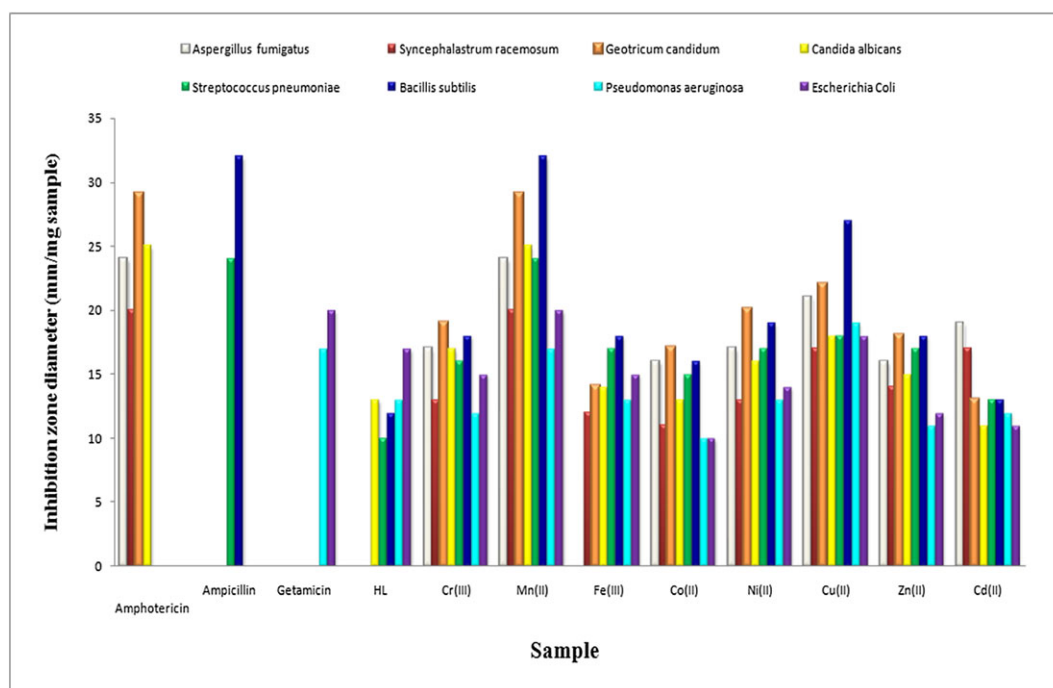


FIGURE 7 Biological activity of HL ligand and its metal complexes

TABLE 5 Biological activity of HL ligand and its metal complexes

Sample	Inhibition zone diameter (mm/mg sample)							
	(Fungi)				Gram (+) Bacteria		Gram (-) Bacteria	
	<i>Aspergillus fumigatus</i>	<i>Syncephalastrum racemosum</i>	<i>Geotricum candidum</i>	<i>Candida albicans</i>	<i>Streptococcus pneumoniae</i>	<i>Bacillus subtilis</i>	<i>Pseudomonas aeruginosa</i>	<i>Escherichia coli</i>
Standard (1): Amphotericin	24	20	29	25	---	---	---	---
Standard (2): Ampicillin	---	---	---	---	24	32	---	---
Standard (3): Getamicin	---	---	---	---	---	---	17	20
HL	0	0	0	13	10	12	13	17
[Cr(L)(Cl)(H ₂ O) ₃]Cl.2H ₂ O	17	13	19	17	16	18	12	15
[Mn(L)(Cl)(H ₂ O) ₃].H ₂ O	24	20	29	25	24	32	17	20
[Fe(L)(Cl)(H ₂ O) ₃]Cl.H ₂ O	0	12	14	14	17	18	13	15
[Co(L)(Cl)(H ₂ O) ₃].H ₂ O	16	11	17	13	15	16	10	10
[Ni(L)(Cl)(H ₂ O) ₃]	17	13	20	16	17	19	13	14
[Cu(L)(Cl)(H ₂ O) ₃]	21	17	22	18	18	27	19	18
[Zn(L)(Cl)(H ₂ O) ₃].2H ₂ O	16	14	18	15	17	18	11	12
[Cd(L)(Cl)(H ₂ O) ₃].3H ₂ O	19	17	13	11	13	13	12	11

estimated weight loss of 37.38% (calcd. 37.95%). Thereafter the weight of the residue corresponds to cadmium oxide contaminated with iron(II) oxide with total weight loss percentage of 66.07% (calcd. 66.68%).

3.3 | Structural interpretation

On the basis of various physico-chemical and spectral data presented and discussed above, the structures of the complexes have been confirmed and the proposed structural formulas of the complexes were shown in Figure 6.

3.3.1 | Antimicrobial activities

Antibacterial activity of the Schiff base ligand and its metal complexes was investigated by a previously reported modified disc diffusion method,^[48] against different bacterial species, such as: two Gram-negative, *Pseudomonas aeruginosa* and *Escherichia coli* and two Gram-positive, *Streptococcus pneumoniae* and *Bacillus subtilis* and against different fungi such as: *Aspergillus fumigatu*, *Syncephalastrum racemosum*, *Geotricum candidum* and *Candida albicans*. The efficiencies of the ligand and the metal complexes have been tested against two Gram (+ve), two Gram (-ve) and four different fungi (Figure 7). The ligand and all complexes have inhibitory action against all microorganisms (Table 5). The metal complexes exhibit higher inhibition against all microorganisms tested compared with free HL ligand.^[49] The biological activity of many ferrocenes increased after the coordination with metal. The rate of

antimicrobial activity of the metal complexes depending on the following five principal factors^[37,50]:

(i) the chelate effect, (ii) the nature of coordinated ligands, (iii) the total charge of the complex, (iv) the nature

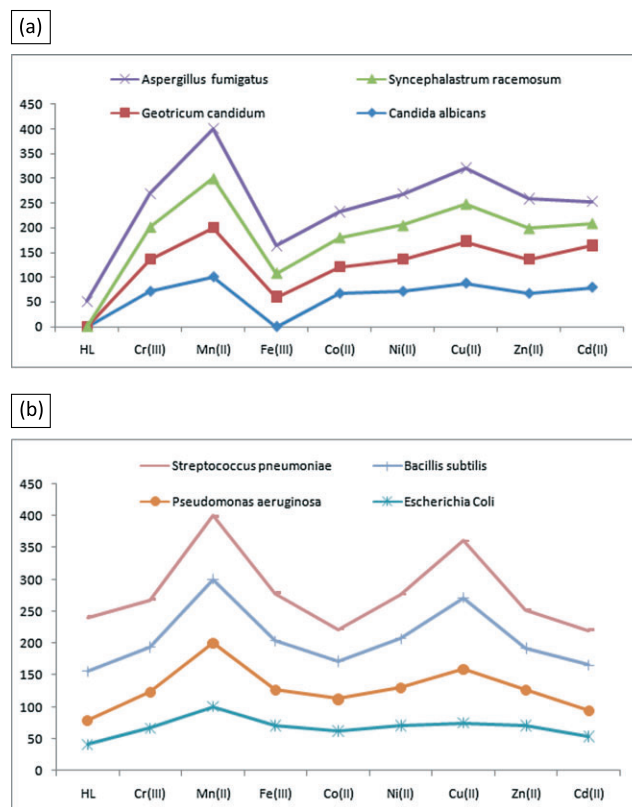


FIGURE 8 Activity index of HL ligand and its metal complexes against (a) different fungal species (b) different bacterial species

of the ion neutralizing the ionic complex, (v) the nuclearity of the metal center in the complex.

Also according to the overtone concept of all permeability, the lipid membrane that surrounds the cell favors the passage of only lipid soluble materials in which liposolubility is an important factor that controls the antimicrobial activity. On chelation the polarity of the metal ion will be reduced to a greater extent due to overlap of ligand orbital and partial sharing of the positive charge of the metal ion with donor groups. Further it increases the delocalization of π -electrons over the whole chelate ring and enhances the lipophilicity of the complexes.^[51] This increased lipophilicity enhances the penetration of the complexes into the lipid membranes and blocks the metal binding sites in enzymes of microorganisms. Finally, the mechanism of action of chemicals and antibiotics against bacteria may be one or more of the followings: Damage of cell wall, inhibition of plasma membrane functions (permeability and energy generation), inhibition of protein synthesis, inhibition of nucleic acids (DNA or

RNA) and Inhibition of enzymes and antimetabolites e.g folic acid synthesis.

The HL-metal complexes of Mn(II), Cu(II) and Ni(II) showed specific antifungal activity of inhibition zone of diameter ranged from 13.0 to 29.0 mm.^[52] All the complexes showed definite bacterial growth inhibition for the four organisms with inhibition zone diameter ranged from 10.0 to 32.0 mm. The results of antimicrobial activities are presented in Table 5. The HL ligand showed activity against the four bacterial organisms in the range of 10.0–17.0 mm^[53]. The Cr(III), Mn(II) and Cu(II) complexes showed the best bacterial inhibition among all the complexes with inhibition zone diameter ranged from 12.0 to 32.0 mm indicating that the coordination of the HL ligand to these metal complexes has enhanced its antimicrobial activity.^[36]

The activities of the prepared ferrocene based Schiff base ligand and its metal complexes were confirmed by calculating the activity index according to the following relation:^[54,55]

TABLE 6 Antibreastic cancer activity of HL ligand and its metal complexes

Complex	Conc. ($\mu\text{g/ml}$)	Surviving fraction (MCF7)					IC ₅₀ ($\mu\text{g/ml}$)
		0.0	5	12.5	25	50	
HL	1	0.944	0.676	0.440	0.276	21.5	
[Cr(L)(Cl)(H ₂ O) ₃].Cl.2H ₂ O	1	0.944	0.840	0.520	0.356	27.7	
[Mn(L)(Cl)(H ₂ O) ₃].H ₂ O	1	0.819	0.561	0.441	0.142	18.7	
[Co(L)(Cl)(H ₂ O) ₃].H ₂ O	1	0.761	0.476	0.333	0.180	11.7	
[Zn(L)(Cl)(H ₂ O) ₃].2H ₂ O	1	0.738	0.523	0.390	0.347	14.7	
[Cd(L)(Cl)(H ₂ O) ₃].3H ₂ O	1	0.904	0.690	0.333	0.214	19.0	

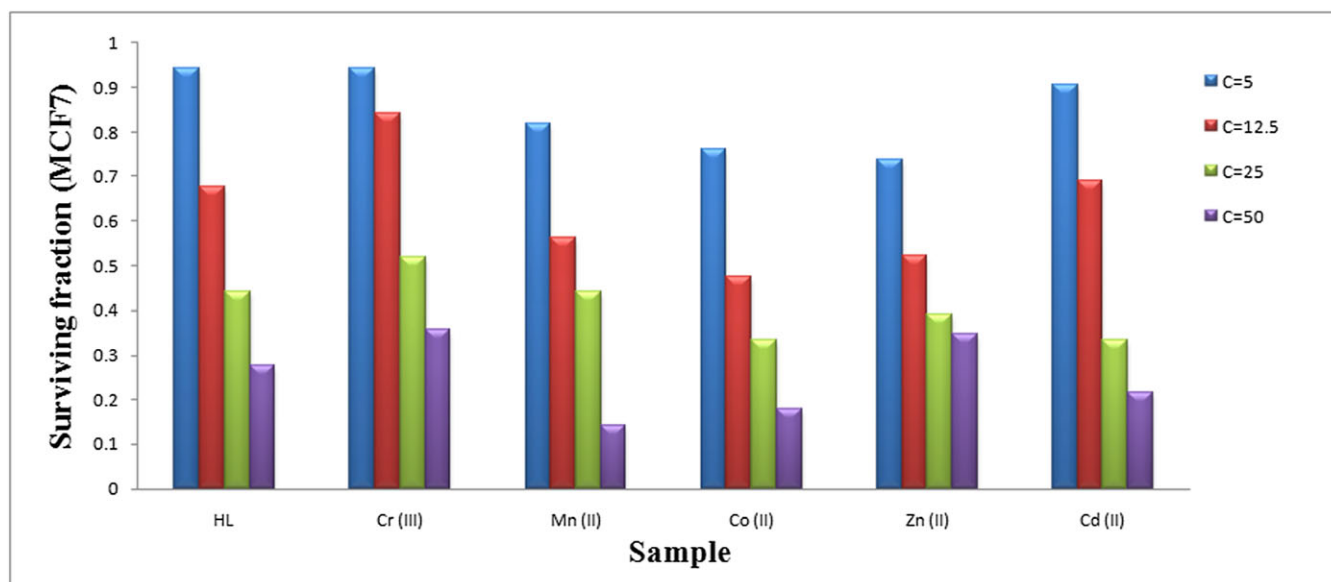


FIGURE 9 Antibreastic cancer activity of HL ligand and its metal complexes

TABLE 7 Energy values obtained in docking calculations of HL with receptors of DNA of human-DNA-Topo I complex (1SC7), the receptors of breast cancer mutant oxidoreductase (3HB5), crystal structure of *Escherichia coli* (3 T88)

Receptor	Ligand moiety	Receptor site	Interaction	Distance (Å ^o)	E (kcal mol ⁻¹)
1SC7	O 18	NZ LYS 493	H-acceptor	2.98	-3.5
	Fe 28	OD1 ASP 533	metal	2.87	-0.7
	C 23	OD1 ASP 533	H-acceptor	3.86	-0.8
3HB5	O 18	N ILE 14	H-acceptor	3.08	-2.6
	Fe 28	O GLY 92	metal	2.09	-1.9
3 T88	O 19	O ASP 67	H-donor	2.82	-2.8
	Fe 28	O ASP 32	metal	2.25	-0.9

$$\text{Activity index (A)} = \frac{\text{Inhibition Zone of compound (mm)}}{\text{Inhibition Zone of standard drug (mm)}} \times 100$$

From the data, it is concluded that Mn(II) complex had the highest activity index, while Fe(III) complex had the lowest activity index, see Figure 8.^[56]

3.3.2 | Anticancer activities

Anticancer activity screening for the tested compounds utilizing four different human tumor cell lines concentrations of breast cancer cell line MCF-7 were obtained from the National Cancer Institute, Cancer Biology Department, Pharmacology Department, Cairo University. The relation between both the surviving fraction and HL ligand concentration was plotted to get the survival curve for each cell line after the specified time. The concentration required for 50% inhibition of cell viability (IC₅₀) was calculated and the results are given in Table 6 and are shown in Figure 9.^[57] From the results, it is clear that Cr(III), Mn(II), Co(II), Zn(II) and Cd(II) complexes are moderately active against breast cancer cells with inhibition ratio of 60–68% against breast cancer cells. It is clear that a pattern of activity can be determined using different ligand concentrations (Table 6 and Figure 9). The IC₅₀ values are found to be 27.7, 18.7, 11.7, 14.7 and 19.0 μg ml⁻¹ for Cr(III), Mn(II), Co(II), Zn(II) and Cd(II) complexes, respectively. It is clear that the cobalt (II) complex has an outstanding IC₅₀ value of 11.7 μg ml⁻¹ and a very low concentration of this complex can be used to produce 50% inhibition of cell growth.^[58]

3.3.3 | Molecular modeling of HL ligand: Docking study

Molecular docking is a key tool in computer drug design.^[59–63] The focus of molecular docking is to simulate the molecular recognition process. Molecular docking aims to achieve an optimized conformation for both the protein and drug with relative orientation between them

such that the free energy of the overall system was minimized. Molecular docking of HL ligand with DNA of human-DNA-Topo I complex (1SC7), the receptors of breast cancer mutant oxidoreductase (3HB5), crystal structure of *Escherichia coli* (3 T88), was performed by the MOE 2008 program suite. The crystal structures of the complexes were used as docking protocols. All hydrogen atoms were added at every inhibitor enzyme interaction^[64] as shown in Figure 8 and the calculated energy was listed in Table 7. According to the results obtained, the Schiff base ligand binds to the proteins with hydrogen bond interactions and decomposed

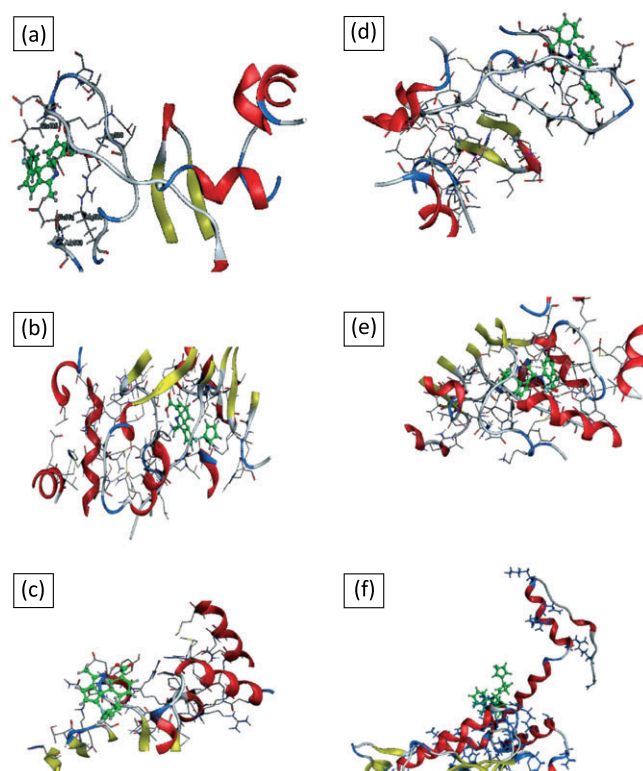
**FIGURE 10** 3D plot of the interaction between HL ligand with receptors of (a) 1Sc7, (b) 3HB5 and (c) 3 T88 and 3D plot of the interaction between [Mn(L⁻)(Cl)(H₂O)₃].H₂O complex with receptors of (d) 1Sc7, (e) 3HB5 and (f) 3 T88

TABLE 8 Energy values obtained in docking calculations of $[\text{Mn}(\text{L}^-)(\text{Cl})(\text{H}_2\text{O})_3]\cdot\text{H}_2\text{O}$ with receptors of DNA of human-DNA-Topo I complex (1SC7), the receptors of breast cancer mutant oxidoreductase (3HB5), crystal structure of *Escherichia coli* (3 T88)

Receptor	Ligand moiety	Receptor site	Interaction	Distance (Å ^o)	E (kcal mol ⁻¹)
1SC7	O 18	NZ LYS 493	H-acceptor	2.98	-3.5
	Fe 28	OD1 ASP 533	metal	2.87	-0.7
	C 23	OD1 ASP 533	H-acceptor	3.86	-0.8
3HB5	O 18	N ILE 14	H-acceptor	3.08	-2.6
	Fe 28	O GLY 92	metal	2.09	-1.9
3 T88	O 19	O ASP 67	H-donor	2.82	-2.8
	Fe 28	O ASP 32	metal	2.25	-0.9

interaction energies in kcal mol⁻¹ exist between HL ligand with 1SC7, 3HB5 and 3 T88 receptors as shown in Figure 10. Three-dimensional plot curves of docking with HL ligand are shown in Figure 10. The Schiff base ligand shows a stronger interaction with 1SC7 receptor than the other receptors.

The binding of HL and its Mn(II) complex with DNA were performed. The minimum binding energies were found to be -3.5 and -3.4 kcal mol⁻¹ for HL and $[\text{Mn}(\text{L})(\text{Cl})(\text{H}_2\text{O})_3]\cdot\text{H}_2\text{O}$, respectively. The minimum energy docked pose revealed that the Mn(II) complexes fitted into the curve contour of the targeted DNA in the groove. Moreover, -OH group of the Mn(II) complex acted as strong H-bond donors or acceptors and were engaged in hydrogen-bonding interactions with O THR 117 in the DNA. The results correlating well with the experiment express that the more polar a compound located at almost the same binding area has, the smaller binding energy is. Molecular docking techniques substantiate the experimental results reported here and at the same time provide further evidence of minor groove binding. It was concluded that the docking study showed a favorable interaction between the HL and its Mn(II) complex and the receptors (1SC7, 3HB5 and 3 T88) as shown in Figure 10 and the calculated energy was listed in Tables 7, 8.

4 | CONCLUSION

Schiff base ligand, HL and its eight new transition metal complexes: Cr(III), Mn(II), Fe(III), Co(II), Ni(II), Cu(II), Zn(II) and Cd(II), with stoichiometry of $[\text{M}(\text{L})\text{Cl}(\text{H}_2\text{O})_3]\cdot\text{xCl}\cdot\text{nH}_2\text{O}$ [M: metals, HL: new ferrocene based Schiff base ligand, n: H₂O and x: chloride] were prepared. All the complexes had been characterized using elemental analysis, FTIR, mass spectroscopy, ¹H-NMR, UV Visible and TGA. The results of antimicrobial assay of ligand and the complexes against some bacteria and fungi suggested the complexes exhibited highest antibacterial as well as antifungal activity. The ligand and its metal ion complexes showed

inhibitory activity against breast carcinoma (MCF7 cell line). In particular, Co(II) and Zn(II) complexes show high anticancer activity with low IC₅₀ values of 11.7 and 14.7 μg ml⁻¹, respectively. Molecular docking studies of the free Schiff base ligand and Mn(II) complex with receptors of (PDB ID: 1SC7, 3HB5 and 3 T88) reveal that HL ligand and Mn(II) complex show highest binding ability (with binding energy of -3.5 and -3.4 kcal mol⁻¹, respectively) with human-DNA-Topo I complex (1SC7) and crystal structure of *Escherichia coli* (3 T88), respectively.

REFERENCES

- [1] C. M. Anderson, S. S. Jain, L. Silber, K. Chen, S. Guha, W. Zhang, E. C. McLaughlin, Y. Hu, J. M. Tanski, *J. Inorg. Biochem.* **2015**, *145*, 41.
- [2] S. S. Jain, C. M. Anderson, F. DiRienzo, I. R. Taylor, K. Jain, S. Guha, N. Hoque, *Chem. Commun.* **2013**, *49*, 5031.
- [3] M. Auzias, J. Gueniat, B. Therrien, G. Süß-Fink, A. K. Renfrew, P. J. Dyson, *J. Organomet. Chem.* **2009**, *694*, 855.
- [4] S. K. Stevens, A. P. Strehle, R. L. Miller, S. H. Gammons, K. J. Hoffman, J. T. McCarty, M. E. Miller, L. K. Stultz, P. K. Hanson, *Mol. Pharmacol.* **2013**, *83*, 225.
- [5] S. Top, A. Vessières, C. Cabestaing, I. Laios, G. Leclercq, C. Provot, G. Jaouen, *J. Organomet. Chem.* **2001**, *637*, 500.
- [6] <https://en.wikipedia.org/wiki/Acetylferrocene>
- [7] M. J. Kelly, R. Tirfoin, J. Gilbert, S. Aldridge, *J. Organomet. Chem.* **2014**, *769*, 11.
- [8] C. R. Wade, A. E. J. Broomsgrove, S. Aldridge, F. P. Gabbai, *Chem. Rev.* **2010**, *110*, 3958.
- [9] M. J. Kelly, A. E. J. Broomsgrove, I. R. Morgan, I. Siewert, P. Fitzpatrick, J. Smart, D. Vidovic, S. Aldridge, *Organometallics* **2013**, *32*, 2674.
- [10] G. Lisa, Y. Yoshitake, T. Michinobu, *J. Anal. Appl. Pyrolysis* **2016**, *120*, 399.
- [11] H. K. H. Yu, L. Wang, W. A. Amer, M. Akram, N. M. Abbasi, Z. u- Abdin, M. Saleem, *Polym. Chem.* **2014**, *5*, 6879.
- [12] I. A. Ansari, F. Sama, M. Raizada, M. Shahid, R. K. Rajpoot, Z. A. Siddiqi, *J. Mol. Struct.* **2017**, *1127*, 479.

- [13] W. H. Mahmoud, N. F. Mahmoud, G. G. Mohamed, A. A. El-Bindary, A. Z. El-Sonbati, *J. Mol. Struct.* **2015**, *1086*, 266.
- [14] A. Z. El-Sonbati, M. A. Diab, A. A. El-Bindary, A. M. Eldesoky, S. M. Morgan, *Spectrochim. Acta A* **2015**, *135*, 774.
- [15] N. A. El-Ghamaz, M. A. Diab, A. A. El-Bindary, A. Z. El-Sonbati, H. A. Seyam, *J. Mater. Sci. Semicond. Proc.* **2014**, *27*, 521.
- [16] A. Albert, *Selective Toxicity*, 6th ed., Wiley, New York **1979**.
- [17] S. Chandra, D. Jain, A. K. Sharma, P. Sharma, *Molecules* **2009**, *14*, 174.
- [18] P. Skehan, R. Storeng, *J. Natl. Cancer Inst.* **1990**, *42*, 1107.
- [19] S. Sangilipandi, D. Sutradhar, K. Bhattacharjee, W. Kaminsky, S. R. Joshi, A. K. Chandra, K. M. Rao, *Inorg. Chim. Acta* **2016**, *441*, 95.
- [20] C. J. Dhanaraj, I. U. Hassan, J. Johnson, J. Joseph, R. S. Joseyphus, *J. Photochem. & Photobio. B: Biology* **2016**, *162*, 115.
- [21] M. Khorshidifard, H. A. Rudbari, Z. Kazemi-Delikani, V. Mirkhani, R. Azadbakht, *J. Mol. Struct.* **2015**, *1081*, 494.
- [22] W. H. Mahmoud, F. N. Sayed, G. G. Mohamed, *Appl. Organomet. Chem.* **2016**, *30*, 959.
- [23] A. Z. El-Sonbati, M. A. Diab, A. A. El-Bindary, S. M. Morgan, *Spectrochim. Acta A* **2014**, *127*, 310.
- [24] N. A. El-Ghamaz, A. Z. El-Sonbati, M. A. Diab, A. A. El-Bindary, M. K. Awad, S. M. Morgan, *Mater. Sci. Semicond. Process.* **2014**, *19*, 150.
- [25] A. Y. Al-Dawood, N. M. El-Metwaly, H. A. El-Ghamry, *J. Mol. Liq.* **2016**, *220*, 311.
- [26] E. Scrocco, J. Tomasi, *Advances in Quantum Chemistry*, Vol. 11, Academic Press, 1st edition Elsevier **1978**, 115.
- [27] F. J. Luque, J. M. Lopez, M. Orozco, *Theor. Chem. Accounts* **2000**, *103*, 343.
- [28] N. Okulik, A. H. Jubert, *Internet Electron J. Mol. Des.* **2005**, *4*, 17.
- [29] D. Rajaraman, G. Sundararajan, N. K. Loganath, K. Krishnasamy, *J. Mol. Struct.* **2017**, *1127*, 597.
- [30] R. Zaky, A. Fekri, Y. G. Abou El-Reash, H. M. Youssef, A. Y. Kareem, *Egyptian J. Basic and Appl. Sci.* **2016**, *3*, 272.
- [31] R. Takjoo, S. S. Hayatolghaibi, H. A. Rudbari, *Inorg. Chim. Acta* **2016**, *447*, 52.
- [32] M. A. Diab, A. Z. El-Sonbati, A. A. El-Bindary, S. M. Morgan, M. K. Abd El-Kader, *J. Mol. Liq.* **2016**, *218*, 571.
- [33] A. A. El-Bindary, G. G. Mohamed, A. Z. El-Sonbati, M. A. Diab, W. M. I. Hassan, S. M. Morgan, A. K. Elkholy, *J. Mol. Liq.* **2016**, *218*, 138.
- [34] S. Altürk, D. Avcı, Ö. Tamer, Y. Atalay, O. Şahin, *J. Phys. Chem. Solid* **2016**, *98*, 71.
- [35] W. H. Mahmoud, R. G. Deghadi, G. G. Mohamed, *J. Therm. Anal. Calorim.* **2017**, *127*, 2149.
- [36] W. H. Mahmoud, M. M. Omar, F. N. Sayed, *J. Therm. Anal. Calorim.* **2016**, *124*, 1071.
- [37] C. J. Dhanaraj, J. Johnson, *Spectrochim. Acta A* **2014**, *118*, 624.
- [38] W. M. I. Hassan, M. A. Badawy, G. G. Mohamed, H. Moustafa, S. Elramly, *Spectrochim. Acta A* **2013**, *111*, 169.
- [39] W. H. Mahmoud, N. F. Mahmoud, G. G. Mohamed, A. A. El-Bindary, A. Z. El-Sonbati, *Spectrochim. Acta A Mol. Biomol. Spectrosc.* **2015**, *150*, 451.
- [40] K. Karaoğlu, M. Emirik, E. Menteşe, A. Zengin, K. Serbest, *Polyhedron* **2016**, *111*, 109.
- [41] S. Y. Ebrahimipour, I. Sheikhshoae, A. C. Kautz, M. Ameri, H. Pasban, H. A. Rudbari, G. Bruno, C. Janiak, *Polyhedron* **2015**, *93*, 99.
- [42] S. M. Pradeepa, H. S. B. Naik, B. V. Kumar, K. I. Priyadarsini, A. Barik, M. C. Prabhakara, *Spectrochim. Acta A* **2015**, *15*, 34.
- [43] W. H. Mahmoud, R. G. Deghadi, G. G. Mohamed, *Appl. Organomet. Chem.* **2016**, *30*, 221.
- [44] R. H. Abu-Eitta, A. H. Bahgat, C. El-Tawil, *Can. J. Chem.* **1985**, *63*, 1173.
- [45] A. Gölcü, P. Yavuz, *Russ. J. Coord. Chem.* **2008**, *34*, 106.
- [46] S. K. Verma, V. K. Singh, *J. Organomet. Chem.* **2015**, *791*, 214.
- [47] J. P. Costes, C. Duhayon, L. Vendier, *Inorg. Chem.* **2014**, *53*, 2181.
- [48] S. Tepavitcharova, D. Havlíček, I. Matulkov, D. Rabadjieva, R. Gergulova, J. Plocek, I. Nemeč, I. Císarov, *J. Mol. Struct.* **2016**, *1120*, 42.
- [49] W. H. Mahmoud, N. F. Mahmoud, G. G. Mohamed, A. Z. El-Sonbati, A. A. El-Bindary, *J. Mol. Struct.* **2015**, *1095*, 15.
- [50] C. M. Sharaby, G. G. Mohamed, M. M. Omar, *Spectrochim. Acta A* **2007**, *66*, 935.
- [51] W. A. Zordok, S. A. Sadeek, *J. Mol. Struct.* **2016**, *1120*, 50.
- [52] H. W. Rossmore, in *Disinfection, Sterilization and Preservation*, fourth ed. (Ed: S. S. Block), Lea and Febinger, Philadelphia **1991**, 290.
- [53] A. D. Russell, in *Disinfection, Sterilization and Preservation*, fourth ed. (Ed: S. S. Block), Lea and Febinger, Philadelphia **1991**, 27.
- [54] I. Muhammad, I. Javed, I. Shahid, I. Nazia, *Turk. J. Biol.* **2007**, *31*, 67.
- [55] T. D. Thangadurai, K. Natarajan, *Indian J. Chem. A* **2001**, *40*, 573.
- [56] Z. H. Chohan, H. Pervez, A. Rauf, K. M. Khan, C. T. Supuran, *J. Enzyme Inhib. Med. Chem.* **2004**, *19*, 417.
- [57] S. Gopalakrishnan, R. Rajameena, E. Vadivel, *Int. J. Pharm. Sci. Drug Res.* **2012**, *4*, 31.
- [58] L. H. Abdel-Rahman, A. M. Abu-Dief, N. A. Hashem, A. A. Seleem, *Int. J. Nano Chem.* **2015**, *1*, 79.
- [59] W. H. Mahmoud, R. G. Deghadi, G. G. Mohamed, *Res. Chem. Intermed.* **2016**, *42*, 7869.
- [60] M. M. Abd-Elzاهر, A. A. Labib, H. A. Mousa, S. A. Moustafa, M. M. Ali, A. A. El Rashedy, *Beni-suef University J. of Basic App. Sci.* **2016**, *5*, 85.
- [61] W. H. Mahmoud, G. G. Mohamed, N. F. Mahmoud, *Appl. Organomet. Chem. I* **2016**, *In press*. <https://doi.org/10.1002/aoc.3583>
- [62] A. Z. El-Sonbati, A. A. El-Bindary, G. G. Mohamed, S. M. Morgan, W. M. I. Hassan, A. K. Elkholy, *J. Mol. Liq.* **2016**, *218*, 16.

- [63] Z. J. Chen, Y. N. Chen, C. N. Xu, S. S. Zhao, Q. Y. Cao, S. S. Qian, J. Qin, H. L. Zhu, *J. Mol. Struct.* **2016**, *1117*, 293.
- [64] B. L. Staker, M. D. Feese, M. Cushman, Y. Pommier, D. Zembower, L. Stewart, A. B. Burgin, *J. Med. Chem.* **2005**, *48*, 2336.

SUPPORTING INFORMATION

Additional Supporting Information may be found online in the supporting information tab for this article.

How to cite this article: Mahmoud WH, Mahmoud NF, Mohamed GG. Synthesis, physicochemical characterization, geometric structure and molecular docking of new biologically active ferrocene based Schiff base ligand with transition metal ions. *Appl Organometal Chem.* 2017;e3858. <https://doi.org/10.1002/aoc.3858>